ACS APPLIED MATERIALS & INTERFACES

Research Article

www.acsami.org

Corallite-like Magnetic Fe_3O_4@MnO_2@Pt Nanocomposites as Multiple Signal Amplifiers for the Detection of Carcinoembryonic Antigen

Dan Wu, Hongmin Ma, Yong Zhang, Hongying Jia, Tao Yan, and Qin Wei*

Key Laboratory of Chemical Sensing & Analysis in Universities of Shandong, School of Chemistry and Chemical Engineering, University of Jinan, Jinan 250022, People's Republic of China

Supporting Information

ABSTRACT: A nonenzymatic sandwich-type electrochemical immunosensor using corallite-like magnetic Fe_3O_4@MnO_2@Pt nanocomposites was developed for the sensitive detection of carcinoembryonic antigen (CEA). First, aminated graphene (GS-NH_2) sheets were synthesized from graphite oxide using the Hummers' method, which was used to immobilize the primary antibody via the active amino groups on the GS-NH_2. Second, corallite-like Fe_3O_4@MnO_2@Pt nanoparticles (NPs) were synthesized and characterized by transmission electron microscope (TEM), scanning electron microscope (SEM), and energy dispersive spectroscopy (EDS). They were used as labels to conjugate with a secondary antibody. The multiple amplification of Fe_3O_4@MnO_2@Pt NPs and the promoted electron transfer of GS-NH_2 lead to a broad linear range from 0.5 pg/mL to 20 ng/mL and a low detection limit with 0.16 pg/mL. In addition, the immunosensor performed with good selectivity and acceptable stability and reproducibility as well. The results are satisfactory when the proposed method has been applied to analyze human serum samples. Thus, there would be a promising future in the early diagnosis of cancer to detect CEA and other tumor markers.

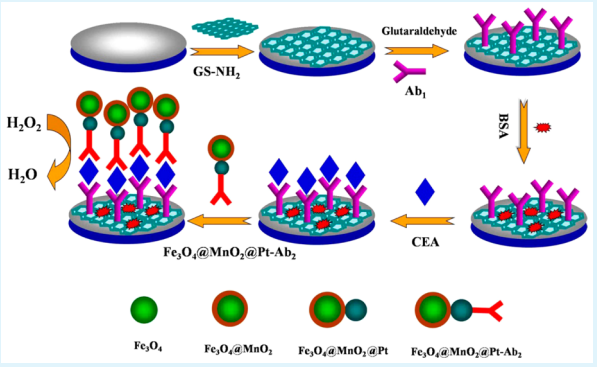

KEYWORDS: *aminated graphene sheets, Fe_3O_4@MnO_2@Pt nanoparticles, carcinoembryonic antigen, electrochemical immunosensor, signal amplification*

INTRODUCTION

Tumor markers, generated by the body in response to cancer growth or by the cancer tissue itself, are proteins. Carcinoembryonic antigen (CEA) is regarded as a preferred tumor marker to predict the outlook for patients having colorectal cancer.[1] The normal range of CEA varies in blood levels among individuals, but the level of an adult without smoking is below 2.5 ng/mL and that of a smoker is less than 5.0 ng/mL.[2] It is necessary to detect CEA with high accuracy and sensitivity in the field of modern biomedicine development.[3] Currently, various immunoassays have been developed to detect tumor markers including the enzyme-linked immunosorbent assay (ELISA),[4] the radioimmunoassay,[5] the electrophoretic immunoassay,[6] the chemiluminescence immunoassay,[7] and the electrochemical immunoassay.[8] Among these methods, the electrochemical immunoassay has attracted more and more interest because of its high selectivity and low detection limit and cost.[9,10] Although great efforts have been made, the highly sensitive and precise detection of CEA using an electrochemical immunosensor is still an important subject to explore. Therefore, developing new labels and strategies to fabricate an electrochemical immunosensor for CEA detection is of great value.

In recent years, Fe_3O_4 nanoparticles (Fe_3O_4 NPs) have received considerable attention for their exploitation in biology and medicine due to their unique properties, including their high stability, variable surface properties, and the magnetic separation method.[11−13] Furthermore, similar to natural peroxidase, Fe_3O_4 is among the limited transition metal oxides that are good catalysts, which is extraordinarily important for an electrochemical immunosensor.[14,15] Hence, a number of biomaterial-functionalized magnetic particles have been widely used in many fields.[16−18] MnO_2 is considered to be a promising electrode material for its high electrocatalytic ability toward H_2O_2, and it has a low cost, is environmentally friendly, and is in natural abundance.[19−21] Furthermore, there is little report regarding the application of MnO_2 in electrochemical immunosensor currently. In the present study, MnO_2 is first used as labels for the immunosensor. The combination of MnO_2 with the Fe_3O_4 NPs successfully improves the current response of the electrochemical immunosensor because it provides the resultant compounds with the synergy of an electric double layer response.

Alternatively, the efficient electrocatalytic ability toward the reduction of H_2O_2 is necessary to construct electrochemical immunosensor for the sensitive detection of CEA. The Pt NPs

Received: June 18, 2015
Accepted: August 5, 2015
Published: August 5, 2015

DOI: 10.1021/acsami.5b05443
ACS Appl. Mater. Interfaces 2015, 7, 18786−18793

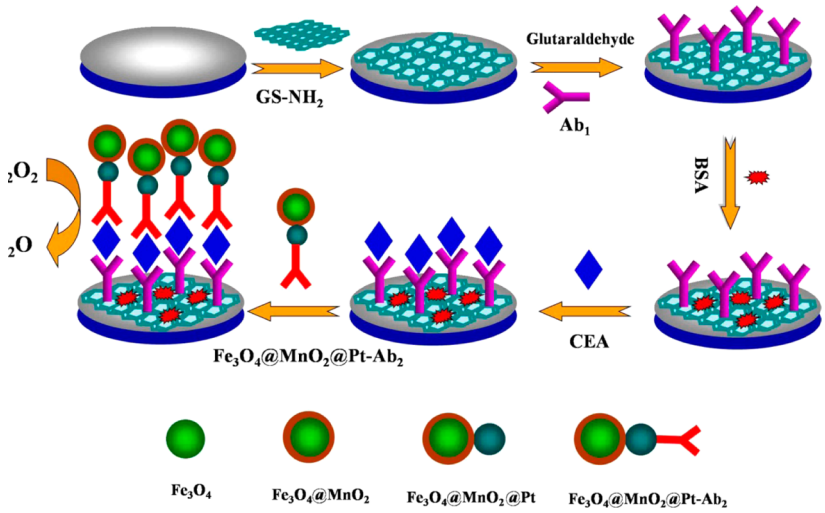

Figure 1. Schematic representation of the preparation process of the immunosensor.

have been extensively used as a catalytic reagent in various chemical reactions, and they not only have exhibited excellent performance in the adsorption and dissociation of H_2O_2 but also have unique catalytic, high specific surface, and electronic properties.[22−25] Additionally, the signal amplification strategy based on the Fe_3O_4@Pt NPs has been applied in the immunosensor by the Yuan group.[15] However, the preparation of Fe_3O_4 with well-dispersed thin-layer MnO_2 sheets and Pt NPs used in the electrochemical immunosensor for better electrochemical performance has not been reported. Therefore, it is crucial to develop a Fe_3O_4@MnO_2@Pt NP-based electrochemical immunosensor for the detection of tumor markers. The as-prepared Fe_3O_4@MnO_2@Pt NPs possess several advantages. First, Fe_3O_4 NPs facilitate magnetic separation and could prevent the loss of the nanoparticles in the period of the washing process. Second, the thin-layer MnO_2 sheets that catalyze H_2O_2 possess a large surface area and can closely interact with the Fe_3O_4 NPs and Pt NPs. Third, the Fe_3O_4@MnO_2@Pt NPs have not only the inherited advantages from the Fe_3O_4, MnO_2, and Pt NPs but also improved properties due to their synergetic effect, which enhances the reduction ability of NPs toward H_2O_2.

Thus, we utilized the unique properties of Fe_3O_4@MnO_2@Pt NPs and aminated graphene ($GS\text{-}NH_2$) sheets to fabricate an electrochemical immunosensor. Because of the synergetic effect between Pt NPs, Fe_3O_4 NPs, and MnO_2 NPs, they could effectively amplify the catalytic reduction toward H_2O_2. Additionally, the $GS\text{-}NH_2$ has good biocompatibility, active amino groups, relatively good solubility, and good electroconductibility.[26,27] By using CEA as the model analyte, the immunosensor exhibited a wide linear range and good selectivity and sensitivity, which indicated that the immunosensor exhibits potential application for the detection of cancer biomarkers.

EXPERIMENTAL SECTION

Reagents and Materials. The CEA, the CEA primary antibody (Ab_1), and the CEA secondary antibody (Ab_2) were purchased from Beijing Dingguo Changsheng Biotechnology Co. Ltd. (China). Bovine serum albumin (BSA, 96−99%) was obtained from Sigma-Aldrich (St. Louis, MO, USA). H_2PtCl_6 was purchased from Alfa Aesar. $K_3[Fe(CN)_6]$, $FeCl_3.6H_2O$, $KMnO_4$, ethylene glycol (EG), NaAc, 2-ethylenediamine (ETH), and graphene were purchased from Sinopharm Chemical Reagent Co., Ltd. (Beijing, China). Phosphate buffered solutions (PBS) were obtained by mixing 0.067 mol/L KH_2PO_4 with 0.067 mol/L Na_2HPO_4 stock solution. Ultrapure water was used throughout the experiments.

Apparatus. The scanning electron microscope (SEM) images were gotten by the field emission SEM (ZEISS, Germany). The transmission electron microscope (TEM) images were investigated with JEM-2100 microscope (JEOL, Tokyo, Japan). Electrochemical measurements were operated by employing a CHI760D electrochemical workstation (Chenhua Instrument Shanghai Co., Ltd., China). A traditional three-electrode system was used including a platinum wire electrode as the auxiliary electrode, a saturated calomel electrode (SCE) as the reference electrode, and a glassy carbon electrode (GCE, 4 mm in diameter) as the working electrode.

Synthesis of $GS\text{-}NH_2$. Graphite oxide (GO) was synthesized using an improved method,[28] and $GS\text{-}NH_2$ was prepared using a reported method.[29] Typically, a 9:1 mixture of concentrated H_2SO_4/H_3PO_4 (360:40 mL) was added to a flask that contained a mixture of graphite (3.0 g, 1 wt %) and $KMnO_4$ (18.0 g, 6 wt %). Then, the reaction was heated to 50 °C and was stirred for 12 h to oxidize the graphite flakes. Next, the reaction was cooled to room temperature and poured slowly onto ice (approximately 400 mL) with 30% H_2O_2 (3 mL). Subsequently, the filtrate was centrifuged (9000 rpm for 20 min). The remaining solid was washed with 200 mL of ultrapure water, 200 mL of 30% HCl, and 200 mL of ethanol 3 times. The material remaining after the preceding wash process was thoroughly washed with 200 mL of ether, and then the obtained solid was dried under vacuum at 35 °C overnight.

The obtained 100 mg of GO solid was added to 40 mL of ethylene glycol during ultrasonication for >0.5 h. Then, after the addition of 1 mL of $NH_3{\cdot}H_2O$ to the preceding mixture, the mixture was transferred to a Teflon-lined autoclave for the solvothermal reaction at 180 °C overnight. Next, the precipitate was filtered, washed thoroughly with doubly distilled water, and dried at 60 °C for 24 h.

Preparation of the Fe_3O_4 NPs. Using the traditional synthesis of Fe_3O_4 NPs,[30] $FeCl_3{\cdot}6H_2O$ (2.7 g) was dissolved in EG (54 mL) to form a clear solution, followed by the addition of NaAc (8.1 g) and ETH (27 mL). The mixture was stirred for 30 min and then sealed in a Teflon-lined stainless steel autoclave. The autoclave was heated to 200 °C, kept for 8 h, and then cooled to room temperature. The black products were washed by means of magnetic separation.

Preparation of the Thin-Layer MnO_2 Nanosheet-Coated Fe_3O_4 NPs (Fe_3O_4@MnO_2 NPs). According to the method provided by Zhang et al.,[31] 20 mL of Fe_3O_4 solution (10 mM) was added to a 250 mL flask containing 100 mL of 0.1 M 2-(*N*-morpholino)-ethanesulfonic acid (MES) buffer (pH 6.0). Then, 60 mL of $KMnO_4$ aqueous solution (10 mM) was added to the flask, and the mixture was sonicated for 40 min until the formation of a brownish black precipitate. After that, the precipitate was isolated using a permanent

DOI: 10.1021/acsami.5b05443
ACS Appl. Mater. Interfaces 2015, 7, 18786−18793

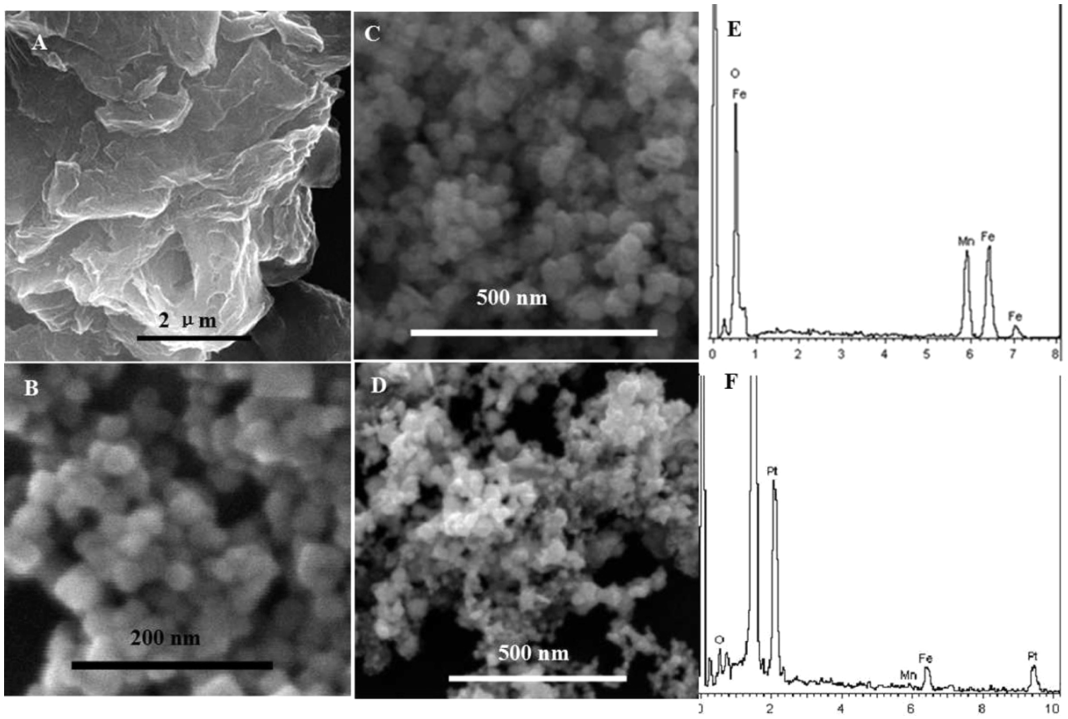

Figure 2. SEM images of the prepared GS-NH_2 (A) and Fe_3O_4 NPs (B); SEM images of the Fe_3O_4@MnO_2 NPs (C) and Fe_3O_4@MnO_2@Pt NPs (D); EDS images of the Fe_3O_4@MnO_2 NPs (E) and Fe_3O_4@MnO_2@Pt NPs (F).

magnet and washed three times with deionized water. Finally, Fe_3O_4@MnO_2 NPs were obtained after being dried at 50 °C for 12 h.

Subsequently, the Fe_3O_4@MnO_2 NPs (1.00 g) were refluxed for 4 h in 80 mL of anhydrous toluene with 1.00 mL of 3-amino-propyltrimethoxysilane to yield the amino-functionalized Fe_3O_4@MnO_2 NPs.

Preparation of the Fe_3O_4@MnO_2@Pt NPs. The preparation of the Fe_3O_4@MnO_2@Pt NPs included the in situ reduction of an improved method.[15] Typically, the as-synthesized Fe_3O_4@MnO_2 NPs (1 mg) were added to a chloroplatinic acid solution (0.01 M, 10 mL) during ultrasonication for 1 h. The mixture was kept in the shaking bath at 25 °C for 12 h so that the chloroplatinic acid absorbed onto the Fe_3O_4@MnO_2 NPs sufficiently. Subsequently, the mixture was separated by magnetic separation, the supernatant was decanted away, and the solid was obtained. Then, the solid was transferred to the flask with 50 mL of doubly distilled water and sodium borohydride (10 mL, 1%). The reactants in the flask were heated for a while, and the solid was obtained by magnetic separation technology again. Finally, the corallite-like Fe_3O_4@MnO_2@Pt NPs were dried at 50 °C in vacuum for 24 h.

Preparation of Fe_3O_4@MnO_2@Pt-Ab_2. The synthesized Fe_3O_4@MnO_2@Pt NPs (1 mg) were dispersed in 1 mL of CTAB (0.018 g) while being stirred for 30 min. Next, PBS at a pH of 7.4 and Ab_2 were added to the preceding mixture, and they were reacted at 4 °C for 12 h during stirring, followed by magnetic separation. The Ab_2 could be immobilized onto the Fe_3O_4@MnO_2@Pt NPs, and the amino groups in the CEA could connect strongly with the Pt NPs.[32] The obtained Fe_3O_4@MnO_2@Pt-Ab_2 were washed with PBS at a pH of 7.4 and then re-dispersed in the PBS and stored at 4 °C before use.

Fabrication of the Immunosensor. Figure 1 shows the fabrication of the sandwich electrochemical immunosensor. The GCE was polished with the use of alumina powder and cleaned thoroughly. First of all, GS-NH_2 was add onto the pretreated GCE and dried. Then, Ab_1 was connected to the GS-NH_2 by glutaraldehyde as the cross-linker of the amino groups. After drying, the electrode was incubated in BSA solution (1%, w/w) for 1 h for eliminating the nonspecific binding effect. Afterward, the CEA solution was dropped onto the surface of the electrode, and 1 h later, the Fe_3O_4@MnO_2@Pt-Ab_2 was adsorbed onto the CEA surface. The immunosensor was incubated for another 1 h, and then it was washed three times to remove any unbound Ab_2. After washing, the prepared electrode was stored at 4 °C prior to use.

Detection of the CEA. For the amperometric measurement of the immunosensor, pH 7.4 PBS was used and −0.4 V was selected as the detection potential. After the background current remained stable under stirring, 5 mM H_2O_2 was injected into the PBS and then the current change was monitored.

RESULTS AND DISCUSSION

Characterization of the GS-NH_2, Fe_3O_4 NPs, the Fe_3O_4@MnO_2 NPs, and the Fe_3O_4@MnO_2@Pt NPs. The Fe_3O_4@MnO_2@Pt NPs were used to label anti-CEA because of their high catalytic properties toward the reduction of H_2O_2. GS-NH_2 with large surface area was used to increase the loading of Ab_1 and to enhance the sensitivity of the proposed immunosensor. Figure 2A shows the morphology of GS-NH_2. From the SEM image of GS-NH_2, we observed that the GS-NH_2 was flake-like, rippled, of an irregular size, and transparent.

The SEM images of the Fe_3O_4 NPs, the Fe_3O_4@MnO_2 NPs, and the Fe_3O_4@MnO_2@Pt NPs are displayed in Figure 2B–D. The Fe_3O_4 NPs have a relatively uniform diameter of ∼40 nm (Figure 2B). Figure 2C shows the surface of the Fe_3O_4 NPs that were covered with amorphous MnO_2 nanosheets, and the average diameter of the Fe_3O_4@MnO_2 NPs was approximately 50 nm. Then, the EDS of the Fe_3O_4@MnO_2 NPs (Figure 2E) further showed that the MnO_2 nanosheets are well-adsorbed on the Fe_3O_4 NPs, and the high specific surface area of Fe_3O_4@MnO_2 NPs endowed sufficient loading of the Pt NPs. The SEM image of the Fe_3O_4@MnO_2@Pt NPs is shown in Figure 2D, and the Pt NPs (bright dots) were adsorbed on the surface of the Fe_3O_4@MnO_2 NPs that obtained corallite-like Fe_3O_4@MnO_2@Pt NPs. Additionally, the EDS of the Fe_3O_4@MnO_2@Pt NPs (Figure 2F) further displayed that the Pt NPs were well-adsorbed on the Fe_3O_4@MnO_2 NP surface.

DOI: 10.1021/acsami.5b05443
ACS Appl. Mater. Interfaces 2015, 7, 18786−18793

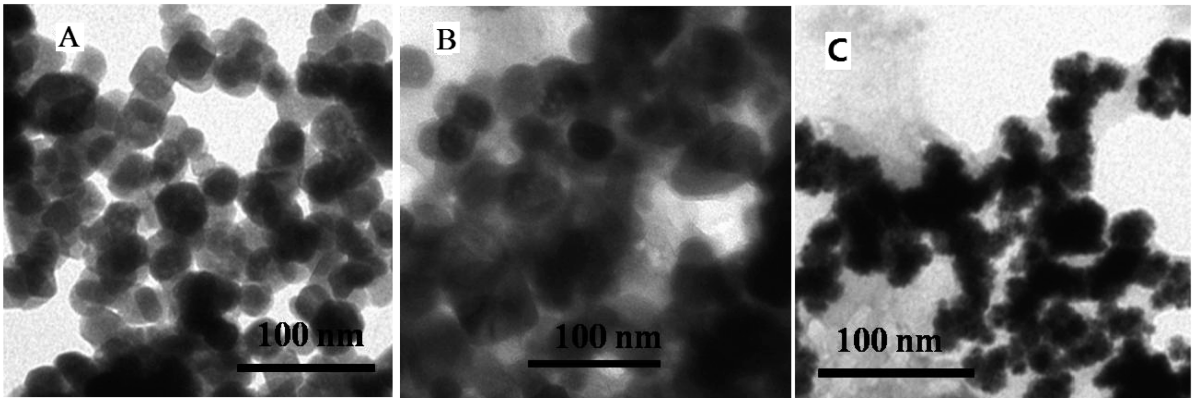

Figure 3. TEM images of the prepared Fe_3O_4 NPs (A), Fe_3O_4@MnO_2 NPs (B), and Fe_3O_4@MnO_2@Pt NPs (C).

The images of Figure 3 exhibit the TEM of Fe_3O_4 NPs, Fe_3O_4@MnO_2 NPs, and Fe_3O_4@MnO_2@Pt NPs, and they could correspond with SEM images and EDS, indicating that Fe_3O_4@MnO_2@Pt NPs have been successfully synthesized.

Characterization of the Immunosensor Using Fe_3O_4@MnO_2@Pt NPs as Labels. For a sandwich-type immunosensor, the sensitivity is primarily determined by the labels used. Herein, the obtained electrochemical signals from the immunosensor are based on the fine electrocatalytic activity of Fe_3O_4@MnO_2@Pt NPs for the reduction of H_2O_2. To obtain their respective electrocatalytic ability, the catalytic performances of Fe_3O_4-Ab_2, Fe_3O_4@MnO_2-Ab_2, Fe_3O_4@Pt-Ab_2, and Fe_3O_4@MnO_2@Pt-Ab_2 for H_2O_2 reduction were investigated. The electrochemical responses of the immunosensor prepared using different labels for detecting 5 ng/mL CEA for H_2O_2 reduction are shown in Figure 4. By using

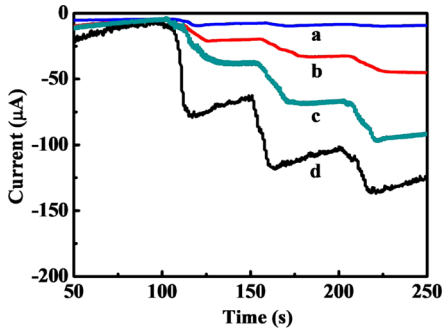

Figure 4. Amperometric responses of the immunosensors for the detection of 5 ng/mL of CEA with different labels toward the addition of 5 mM H_2O_2 in pH 7.4 PBS: (a) Fe_3O_4-Ab_2, (b) Fe_3O_4@MnO_2-Ab_2, (c) Fe_3O_4@Pt-Ab_2, and (d) Fe_3O_4@MnO_2@Pt-Ab_2.

Fe_3O_4-Ab_2 as the label, the immunosensor had a current response (curve a) for the catalytic ability of Fe_3O_4. For the immunosensor using Fe_3O_4@MnO_2-Ab_2 as the label, there is a large current response (curve b), which indicated that MnO_2 could catalyze H_2O_2 well, and the synthesis of Fe_3O_4@MnO_2 was sufficient. When Fe_3O_4@Pt-Ab_2 was used as the label in the immunosensor, a larger current response (curve c) occurred, indicating that Pt NPs could catalyze H_2O_2 sufficiently. When using Fe_3O_4@MnO_2@Pt-Ab_2 as the labels, the immunosensor displayed the largest current response (curve d). These results show that the immunosensor that used Fe_3O_4@MnO_2@Pt-Ab_2 as the labels exhibited good catalytic performance toward H_2O_2 due to the multiple signal amplification of the Pt NPs, the MnO_2 NPs, and the Fe_3O_4 NPs.

Characterization of the Immunosensor. Electrochemical impedance spectra (EIS) were used to monitor the electrochemical property of the immunosensor during the fabrication process.[33] There is a semicircle and a linear portion in the impedance spectra. The linear portion is associated with the diffusion process, and the semicircle diameter corresponds to the electron-transfer resistance. Considering the stepwise assembly and coating involved in the immunosensor, the fabrication process was elucidated for a comparative study. The impedance spectra in the presence of 5.0 mmol/L $[Fe(CN)_6]^{3-/4-}$ solution containing 0.1 mol/L KCl were recorded in the frequency range from 0.1 to 10^5 Hz at 0.167 V (vs Ag/AgCl). The amplitude of the alternating voltage was 5 mV. It can be seen from the EIS (Figure 5A), the bare GCE (curve a) displays a very small semicircle domain. After the modification of the GS-NH_2 onto the electrode (curve b), the curve is almost linear. The result shows that GS-NH_2, as an excellent electrically conducting material, makes the electron-transfer process easier. After the electrode was coated by glutaraldehyde, reinforcement of the semicircle portions was obtained (curves c). After adding Ab_1 onto the electrode, the resistance was increased (curve d), which indicated the successful immobilization of Ab_1 onto the electrode. Then, a larger semicircle was found, indicating that the high resistance of the electrode interface was hindered by BSA (curve e). After that, the resistance increased again (curve f), clarifying the successful capture of CEA. When the Fe_3O_4@MnO_2@Pt-Ab_2 NPs were further incubated on the electrode, the resistance reached the maximum (curve g), which indicated that the assembly process of the electrode was successful.

The equivalent circuit, containing the charge-transfer resistance (R_{ct}), the resistance of solution (R_s), the double layer capacitance (C_{dl}), and the Warburg impedance (Z_W), is displayed in Figure 5A (shown by inset). And the corresponding values fitted by using ZSimpwin software are listed in Table S1. During the electrode modification processes, the changes in R_{ct} were more significant than other impedance components. Therefore, R_{ct} is selected suitably as a signal for sensing the interfacial properties of the modified GCE.

The modified electrodes were further characterized by cyclic voltammetry (CV). CVs of the different modified electrodes were scanned for 2 cycles from −0.2 to 0.6 V in 5.0 mmol/L $K_3[Fe(CN)_6]$ solution containing 0.1 mol/L KCl. The scan rate was 100 mV/s. The peak potentials and peak currents remained very stable after the second cycle. Thus, the second cycle was

DOI: 10.1021/acsami.5b05443
ACS Appl. Mater. Interfaces 2015, 7, 18786−18793

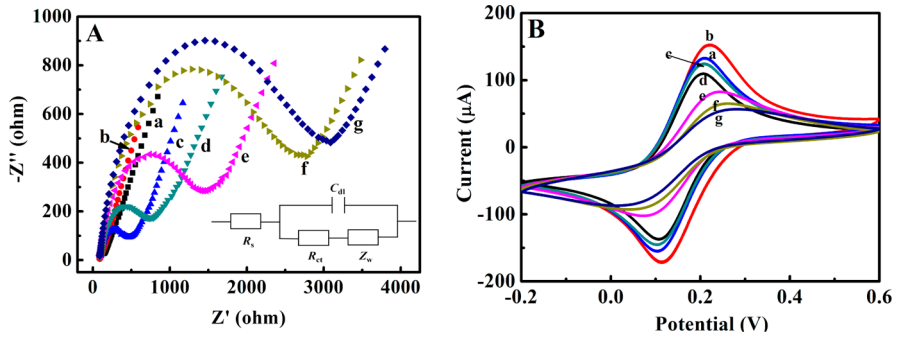

Figure 5. EIS in the presence of 5.0 mmol/L $[Fe(CN)_6]^{3-/4-}$ solution containing 0.1 mol/L KCl (A) and CVs scanned from −0.2 V to 0.6 V in 5.0 mmol/L $K_3[Fe(CN)_6]$ containing 0.1 mol/L KCl with a scan rate of 100 mV/s (B) obtained for each immobilized step: (a) GCE, (b) GCE/GS-NH_2, (c) GCE/GS-NH_2/glutaraldehyde, (d) GCE/GS-NH_2/glutaraldehyde/Ab_1, (e) GCE/GS-NH_2/glutaraldehyde/Ab_1/BSA, (f) GCE/GS-NH_2/glutaraldehyde/Ab_1/BSA/CEA, and (g) GCE/GS-NH_2/glutaraldehyde/Ab_1/BSA/CEA/Fe_3O_4@MnO_2-Pt-Ab_2.

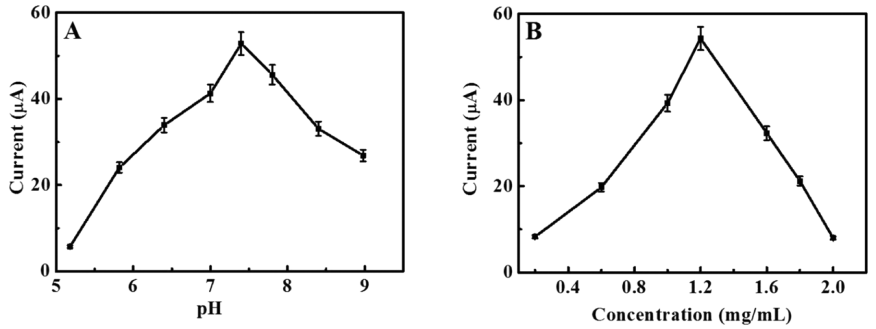

Figure 6. Effect of pH (A) and GS-NH_2 concentration (B) on the current change of the immunosensor during the detection of 5 ng/mL CEA in 10 mL of PBS that contained 5 mM H_2O_2.

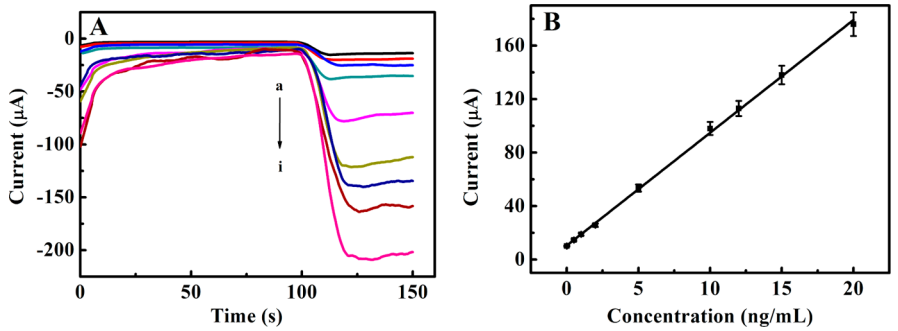

Figure 7. Amperometric response (A) and calibration curve (B) of the immunosensor for the detection of different concentrations of CEA (a) 0.0005, (b) 0.01, (c) 0.5, (d) 1, (e) 5, (f) 10, (g) 12, (h) 15, and (i) 20 ng/mL. Error bar = RSD (n = 5).

used to draw the cyclic voltammogram, and the results are shown in Figure 5B. A pair of well-defined reduction/oxidation peaks were observed at the bare GCE (curve a). After the modification of GS-NH_2 (curve b), the peak current was much higher than that of GCE. Then, the peak current decreased gradually with the addition of glutaraldehyde (curve c), Ab_1 (curve d), BSA (curve e), CEA (curve f), and Fe_3O_4@MnO_2@Pt-Ab_2 (curve g). The preceding results are consistent with the changes observed in the charge-transfer resistance by EIS.

Optimization of the Experimental Conditions. To get the sensitive CEA detection, the experimental conditions required optimization. PBS that contained 5 mM H_2O_2 covering the pH range from 5.2 to 9.0 was used to study the effect of pH on the current response at 5 ng/mL of CEA. As shown in Figure 6A, the current increased from pH 5.2 to 7.4, and then it decreased. Therefore, pH 7.4 PBS was used throughout this study.

The amount of GS-NH_2 is another key parameter that affects the loading amount of Ab_1 and the electrochemical behaviors of the GS-NH_2. When GS-NH_2 concentration increased from 0.2 to 2 ng/mL (shown in Figure 6B), the current response of the immunosensor increased at first and then decreased. So 1.2 ng/mL GS-NH_2 was selected as the suitable concentration.

Performance of the Immunosensors. Because the high sensitivity of the immunosensor using Fe_3O_4@MnO_2@Pt as the label has been verified, a great deal of Ab_2 was fixed onto the Fe_3O_4@MnO_2@Pt. Hence, in the presence of CEA on the electrode, Fe_3O_4@MnO_2@Pt-Ab_2 labels could be easily captured onto the electrode surface through antibody−antigen interaction, and the amount of label captured is proportional to the CEA concentration. Therefore, the immunosensor could be used for the quantification of CEA. As displayed in Figure 7A,B, the current response increased with the increasing of CEA concentration from 0.5 pg/mL to 20 ng/mL, and the equation

DOI: 10.1021/acsami.5b05443
ACS Appl. Mater. Interfaces 2015, 7, 18786−18793

Table 1. Comparisons of Proposed Method with Other Reported Electrochemical Immunosensors for CEA

electrode materials	linear range	detection limit	reference
hyperbranched polyester	0.01−80 ng/mL	2.36 pg/mL	34
Au/PDCNTs/$(PSS/PDCNTs)_2$	0.1−2.0 ng/mL	0.06 ng/mL	35
	2.0−160 ng/mL		
Nafion-cysteine/Au NPs	0.01−100 ng/mL	3.3 pg/mL	36
AuNPs/Thi-CNTs	0.02−80 ng/mL	0.008 ng/mL	37
Thi@NPG/AuNPs	10 pg/mL to 100 ng/mL	3 pg/mL	38
OPD/CS/nano-Au	0.008−200 ng/mL	5 pg/mL	39
GS-NH_2	0.5 pg/mL to 20 ng/mL	0.16 pg/mL	this work

of the calibration curve for the immunosensor was $Y/\mu A = 8.180(X/(ng/mL)) + 12.25$. The detection limit was 0.16 pg/mL. Compared with the analytical characteristics of other CEA immunosensors including the detection limit and linear range (Table 1), the proposed method is better or comparable to the results reported. The reason may be ascribed to three factors: (1) owing to the high surface area of GS-NH_2, the loading of Ab_1 could significantly be increased, and (2) the high catalytic activity of Fe_3O_4@MnO_2@Pt NPs toward H_2O_2 and (3) the good magnetism of Fe_3O_4 made the separation and washing processes easy.

Reproducibility, Selectivity, and Stability of the Immunosensor. To access the reproducibility of the immunosensor, five electrodes were prepared to detect 5 ng/mL of CEA. After measuring the five electrodes, the relative standard deviation (RSD) was 2.7%, which means good reproducibility for the proposed immunosensor.

The selectivity was also tested. A CEA (5 ng/mL) solution that contained 1000 ng/mL of interfering substances including CA-125, AFP, vitamin C, glucose, and BSA was prepared and measured by the preceding method, respectively. The current variation caused by the interfering substances was 2.3%, and the selectivity was proved to be acceptable.

The stability of the immunosensor was studied periodically. When the immunosensor was prepared and not in use, it was stored at 4 °C. The current of the immunosensor was decreased to 92% and 86% of its initial response after 1 week and 3 weeks, respectively.

Real Sample Analysis. The preceding immunosensor was used to determine the recoveries of different concentrations of CEA in human serum by standard addition methods in order to access the feasibility for possible applications. As shown in Table 2, the recoveries were 98.7%, 106%, and 94.9%. The results indicate that the proposed immunosensor supplies a promising approach for clinical research and diagnostic applications.

Table 2. Results for the Detection of CEA in Serum by the Prepared Immunosensor

content of CEA in the serum sample (ng/mL)	addition content (ng/mL)	detection content (ng/mL)	av value (ng/mL)	recovery (%)
2.35	1.50	3.76, 3.78, 3.83, 3.87, 3.86	3.82	98.7
	3.50	5.93, 5.82, 6.00, 6.06, 6.13	5.99	106
	6.50	8.58, 8.64, 8.71, 8.86, 8.88	8.73	94.9

Meanwhile, ELISA method was used as a reference method to validate the proposed method. By using ELISA method and the proposed methods, the CEA concentration in human serum sample was determined 5 times, respectively. The results are shown in Table S2. The relative error between the two methods was 3.1%. Based on the *F*-test, the *F* calculated is less than the theoretical value, indicating that the precisions were not obviously different from those obtained by ELISA method. According to the *t*-test, the mean values were also not remarkably different from those obtained by ELISA method, indicating that there is no system error in this method. These data proved a good agreement between the two methods and presented sufficient precision and high accuracy.

CONCLUSIONS

A sandwich electrochemical immunosensor was easily developed by using GS-NH_2 to immobilize Ab_1 and utilize Fe_3O_4@MnO_2@Pt NPs as the labels for the CEA detection. To construct the high-performance electrochemical immunosensor, Fe_3O_4@MnO_2@Pt NPs were used as the labels, and the labels enhanced the reduction ability of NPs toward H_2O_2. Hence, the obtained immunosensor exhibited good reproducibility, high selectivity, and acceptable stability. This new and simple sandwich-type immunosensor is a valuable method in the field of clinical detection.

ASSOCIATED CONTENT

Supporting Information

The Supporting Information is available free of charge on the ACS Publications website at DOI: 10.1021/acsami.5b05443.

Simulation parameters of the equivalent circuit components and comparisons of the developed method with the ELISA method (PDF)

AUTHOR INFORMATION

Corresponding Author

*Tel.: +86 531 82765730. Fax: +86 531 82765969. E-mail: sdjndxwq@163.com.

Notes

The authors declare no competing financial interest.

ACKNOWLEDGMENTS

This study was supported by the Natural Science Foundation of China (Grant Nos. 21375047, 21377046, and 21405059), Shandong Province (Grant No. ZR2014BL024), and the Science and Technology Plan Project of Jinan (Grant No. 201307010). Q.W. also thanks the Special Foundation for Taishan Scholar Professorship of Shandong Province and UJN (Grant No. ts20130937).

DOI: 10.1021/acsami.5b05443
ACS Appl. Mater. Interfaces 2015, 7, 18786−18793

REFERENCES

(1) Zhou, J.; Zhuang, J. Y.; Miró, M.; Gao, Z.; Chen, G.; Tang, D. Carbon Nanospheres-Promoted Electrochemical Immunoassay Coupled with Hollow Platinum Nanolabels for Sensitivity Enhancement. *Biosens. Bioelectron.* **2012**, *35*, 394−400.

(2) Yang, H.; Yuan, R.; Chai, Y.; Mao, L.; Su, H.; Jiang, W.; Liang, M. Electrochemical Immunosensor for Detecting Carcinoembryonic Antigen Using Hollow Pt Nanospheres-Labeled Multiple Enzyme-Linked Antibodies As Labels For Signal Amplification. *Biochem. Eng. J.* **2011**, *56*, 116−124.

(3) Zhou, J.; Tang, J.; Chen, G.; Tang, D. Layer-By-Layer Multienzyme Assembly for Highly Sensitive Electrochemical Immunoassay Based on Tyramine Signal Amplification Strategy. *Biosens. Bioelectron.* **2014**, *54*, 323−328.

(4) Dixit, C. K.; Vashist, S. K.; O'neill, F. T.; O'reilly, B.; Maccraith, B. D.; O'kennedy, R. Development of a High Sensitivity Rapid Sandwich ELISA Procedure and Its Comparison with the Conventional Approach. *Anal. Chem.* **2010**, *82*, 7049−7052.

(5) Rubery, E.; Doran, J.; Thompson, R. Brain-Type Creatine Kinase BB As A Potential Tumour Marker-Serum Levels Measured by Radioimmunoassay in 1015 Patients with Histologically Confirmed Malignancies. *Eur. J. Cancer Clin. Oncol.* **1982**, *18*, 951−956.

(6) He, Z.; Gao, N.; Jin, W. Determination of Tumor Marker CA125 by Capillary Electrophoretic Enzyme Immunoassay with Electrochemical Detection. *Anal. Chim. Acta* **2003**, *497*, 75−81.

(7) Lee, J. S.; Joung, H.-A.; Kim, M.-G.; Park, C. B. Graphene-Based Chemiluminescence Resonance Energy Transfer for Homogeneous Immunoassay. *ACS Nano* **2012**, *6*, 2978−2983.

(8) Wu, D.; Fan, H.; Li, Y.; Zhang, Y.; Liang, H.; Wei, Q. Ultrasensitive Electrochemical Immunoassay for Squamous Cell Carcinoma Antigen Using Dumbbell-Like Pt−Fe_3O_4 Nanoparticles as Signal Amplification. *Biosens. Bioelectron.* **2013**, *46*, 91−96.

(9) Tang, J.; Tang, D.; Niessner, R.; Chen, G.; Knopp, D. Magneto-Controlled Graphene Immunosensing Platform for Simultaneous Multiplexed Electrochemical Immunoassay Using Distinguishable Signal Tags. *Anal. Chem.* **2011**, *83*, 5407−5414.

(10) Zhang, X.; Li, F.; Wei, Q.; Du, B.; Wu, D.; Li, H. Ultrasensitive Nonenzymatic Immunosensor Based on Bimetallic Gold−Silver Nanoclusters Synthesized by Simple Mortar Grinding Route. *Sens. Actuators, B* **2014**, *194*, 64−70.

(11) Wang, H.; Yuan, X.; Wu, Y.; Chen, X.; Leng, L.; Wang, H.; Li, H.; Zeng, G. Facile Synthesis of Polypyrrole Decorated Reduced Graphene Oxide−Fe_3O_4 Magnetic Composites and Its Application For The Cr(Vi) Removal. *Chem. Eng. J.* **2015**, *262*, 597−606.

(12) Ghaemi, N.; Madaeni, S. S.; Daraei, P.; Rajabi, H.; Zinadini, S.; Alizadeh, A.; Heydari, R.; Beygzadeh, M.; Ghouzivand, S. Polyethersulfone Membrane Enhanced With Iron Oxide Nanoparticles for Copper Removal from Water: Application of New Functionalized Fe_3O_4 Nanoparticles. *Chem. Eng. J.* **2015**, *263*, 101−112.

(13) Parshetti, G. K.; Lin, F.-H.; Doong, R.-A. Sensitive Amperometric Immunosensor for A-Fetoprotein Detection Based on Multifunctional Dumbbell-Like Au-Fe_3O_4 Heterostructures. *Sens. Actuators, B* **2013**, *186*, 34−43.

(14) Backmann, N.; Zahnd, C.; Huber, F.; Bietsch, A.; Plückthun, A.; Lang, H.-P.; Güntherodt, H.-J.; Hegner, M.; Gerber, C. A Label-Free Immunosensor Array Using Single-Chain Antibody Fragments. *Proc. Natl. Acad. Sci. U. S. A.* **2005**, *102*, 14587−14592.

(15) Yang, Z.; Chai, Y.; Yuan, R.; Zhuo, Y.; Li, Y.; Han, J.; Liao, N. Hollow Platinum Decorated Fe_3O_4 Nanoparticles as Peroxidase Mimetic Couple With Glucose Oxidase for Pseudobienzyme Electrochemical Immunosensor. *Sens. Actuators, B* **2014**, *193*, 461−466.

(16) Peng, H.-P.; Liang, R.-P.; Zhang, L.; Qiu, J.-D. Sonochemical Synthesis of Magnetic Core−Shell Fe_3O_4@ZrO_2 Nanoparticles and Their Application to the Highly Effective Immobilization of Myoglobin for Direct Electrochemistry. *Electrochim. Acta* **2011**, *56*, 4231−4236.

(17) Liu, Y.; Han, T.; Chen, C.; Bao, N.; Yu, C.-M.; Gu, H.-Y. A Novel Platform of Hemoglobin on Core−Shell Structurally Fe_3O_4@Au Nanoparticles and Its Direct Electrochemistry. *Electrochim. Acta* **2011**, *56*, 3238−3247.

(18) Samanta, B.; Yan, H.; Fischer, N. O.; Shi, J.; Jerry, D. J.; Rotello, V. M. Protein-Passivated Fe_3O_4 Nanoparticles: Low Toxicity and Rapid Heating for Thermal Therapy. *J. Mater. Chem.* **2008**, *18*, 1204−1208.

(19) Ren, Y.; Xu, Q.; Zhang, J.; Yang, H.; Wang, B.; Yang, D.; Hu, J.; Liu, Z. Functionalization of Biomass Carbonaceous Aerogels: Selective Preparation of MnO_2@CA Composites for Supercapacitors. *ACS Appl. Mater. Interfaces* **2014**, *6*, 9689−9697.

(20) Zhu, J.; Tang, S.; Xie, H.; Dai, Y.; Meng, X. Hierarchically Porous MnO_2 Microspheres Doped with Homogeneously Distributed Fe_3O_4 Nanoparticles for Supercapacitors. *ACS Appl. Mater. Interfaces* **2014**, *6*, 17637−17646.

(21) Yu, G.; Hu, L.; Vosgueritchian, M.; Wang, H.; Xie, X.; Mcdonough, J. R.; Cui, X.; Cui, Y.; Bao, Z. Solution-Processed Graphene/MnO_2 Nanostructured Textiles for High-Performance Electrochemical Capacitors. *Nano Lett.* **2011**, *11*, 2905−2911.

(22) Liang, H.-P.; Zhang, H.-M.; Hu, J.-S.; Guo, Y.-G.; Wan, L.-J.; Bai, C.-L. Pt Hollow Nanospheres: Facile Synthesis and Enhanced Electrocatalysts. *Angew. Chem., Int. Ed.* **2004**, *43*, 1540−1543.

(23) Bai, L.; Yuan, R.; Chai, Y.; Yuan, Y.; Zhuo, Y.; Mao, L. Bi-Enzyme Functionlized Hollow Ptco Nanochains as Labels for an Electrochemical Aptasensor. *Biosens. Bioelectron.* **2011**, *26*, 4331−4336.

(24) You, T.; Niwa, O.; Tomita, M.; Hirono, S. Characterization of Platinum Nanoparticle-Embedded Carbon Film Electrode and Its Detection of Hydrogen Peroxide. *Anal. Chem.* **2003**, *75*, 2080−2085.

(25) Teng, X.; Liang, X.; Maksimuk, S.; Yang, H. Synthesis of Porous Platinum Nanoparticles. *Small* **2006**, *2*, 249−253.

(26) Li, N.; Wang, Y.; Li, Y.; Cao, W.; Ma, H.; Wu, D.; Du, B.; Wei, Q. A Label-Free Electrochemical Immunosensor Based on Au@Pd/Ag Yolk-Bimetallic Shell Nanoparticles and Amination Graphene for Detection of Nuclear Matrix Protein 22. *Sens. Actuators, B* **2014**, *202*, 67−73.

(27) Ren, X.; Yan, T.; Zhang, Y.; Wu, D.; Ma, H.; Li, H.; Du, B.; Wei, Q. Nanosheet Au/Co_3O_4-Based Ultrasensitive Nonenzymatic Immunosensor for Melanoma Adhesion Molecule Antigen. *Biosens. Bioelectron.* **2014**, *58*, 345−350.

(28) Marcano, D. C.; Kosynkin, D. V.; Berlin, J. M.; Sinitskii, A.; Sun, Z.; Slesarev, A.; Alemany, L. B.; Lu, W.; Tour, J. M. Improved Synthesis of Graphene Oxide. *ACS Nano* **2010**, *4*, 4806−4814.

(29) Lai, L.; Chen, L.; Zhan, D.; Sun, L.; Liu, J.; Lim, S. H.; Poh, C. K.; Shen, Z.; Lin, J. One-Step Synthesis of NH_2-Graphene from in Situ Graphene-Oxide Reduction and Its Improved Electrochemical Properties. *Carbon* **2011**, *49*, 3250−3257.

(30) Guo, S.; Li, D.; Zhang, L.; Li, J.; Wang, E. Monodisperse Mesoporous Superparamagnetic Single-Crystal Magnetite Nanoparticles for Drug Delivery. *Biomaterials* **2009**, *30*, 1881−1889.

(31) Zhang, L.; Lian, J.; Wu, L.; Duan, Z.; Jiang, J.; Zhao, L. Synthesis of a Thin-Layer MnO_2 Nanosheet-Coated Fe_3O_4 Nanocomposite as a Magnetically Separable Photocatalyst. *Langmuir* **2014**, *30*, 7006−7013.

(32) Mandal, S.; Roy, D.; Chaudhari, R. V.; Sastry, M. Pt And Pd Nanoparticles Immobilized on Amine-Functionalized Zeolite: Excellent Catalysts for Hydrogenation and Heck Reactions. *Chem. Mater.* **2004**, *16*, 3714−3724.

(33) Ho, M. Y.; D'souza, N.; Migliorato, P. Electrochemical Aptamer-Based Sandwich Assays for the Detection of Explosives. *Anal. Chem.* **2012**, *84*, 4245−4247.

(34) Miao, J.; Wang, X.; Lu, L.; Zhu, P.; Mao, C.; Zhao, H.; Song, Y.; Shen, J. Electrochemical Immunosensor Based on Hyperbranched Structure for Carcinoembryonic Antigen Detection. *Biosens. Bioelectron.* **2014**, *58*, 9−16.

(35) Gao, X.; Zhang, Y.; Chen, H.; Chen, Z.; Lin, X. Amperometric Immunosensor for Carcinoembryonic Antigen Detection with Carbon Nanotube-Based Film Decorated with Gold Nanoclusters. *Anal. Biochem.* **2011**, *414*, 70−76.

(36) Liao, Y.; Yuan, R.; Chai, Y.; Zhuo, Y.; Yang, X. Study on an Amperometric Immunosensor Based on Nafion−Cysteine Composite

DOI: 10.1021/acsami.5b05443
ACS Appl. Mater. Interfaces 2015, 7, 18786−18793

Membrane for Detection of Carcinoembryonic Antigen. *Anal. Biochem.* **2010**, *402*, 47−53.
(37) Feng, D.; Li, L.; Fang, X.; Han, X.; Zhang, Y. Dual Signal Amplification of Horseradish Peroxidase Functionalized Nanocomposite as Trace Label for the Electrochemical Detection of Carcinoembryonic antigen. *Electrochim. Acta* **2014**, *127*, 334−341.
(38) Sun, X.; Ma, Z. Electrochemical Immunosensor Based on Nanoporpus Gold Loading Thionine for Carcinoembryonic Antigen. *Anal. Chim. Acta* **2013**, *780*, 95−100.
(39) Gan, N.; Jia, L.; Zheng, L. A Sandwich Electrochemical Immunosensor Using Magnetic DNA Nanoprobes for Carcinoembryonic Antigen. *Int. J. Mol. Sci.* **2011**, *12*, 7410−7423.

DOI: 10.1021/acsami.5b05443
ACS Appl. Mater. Interfaces 2015, 7, 18786−18793